ЖЭТФ, 2007, том 132, вып. 6 (12), стр. 1359–1367

KINETICS OF THE SPIN-2 BLUME–CAPEL MODEL UNDER A TIME-DEPENDENT OSCILLATING EXTERNAL FIELD

M. Keskin [a*], ***O. Canko*** [a**], ***M. Ertaş*** [b***]

[a] *Department of Physics, Erciyes University 38039, Kayseri, Turkey*

[b] *Institute of Science, Erciyes University 38039, Kayseri, Turkey*

Received April 12, 2007

Within a mean-field approach and using the Glauber-type stochastic dynamics, we study the kinetics of the spin-2 Blume–Capel model in the presence of a time-varying (sinusoidal) magnetic field. We investigate the time dependence of the average order parameter and the behavior of the average order parameter in a period, which is also called the dynamic order parameter, as a function of the reduced temperature. The nature (continuous and discontinuous) of a transition is characterized by the dynamic order parameter. The dynamic phase transition points are obtained and the phase diagrams are presented in the reduced magnetic field amplitude and reduced temperature plane. The phase diagrams exhibit one dynamic tricritical point; besides a disordered and one ordered phases, there are three phase coexistence regions that are strongly dependent on the interaction parameter.

PACS: 05.50.+q, 05.70.Fh, 64.60.Ht, 75.10.Hk

1. INTRODUCTION

Spin-1 and spin-3/2 systems have been one of the most actively studied models in statistical mechanics and condensed matter physics; they have been used as elementary models for a variety of phenomena for several decades. Recently, sustained research effort has been exerted in investigating equilibrium properties of the spin-2 Ising model. An early attempt to study the one-dimensional Ising model for $S = 2$ (also $S = 1$ and $3/2$) was made in [1] by generalizing the Bethe approximation. The authors only calculated the energy and the specific heat exactly. The dipolar and quadrupolar ordering in the spin-2 doublet–triplet system was studied in the molecular field approximation in [2]. The cluster variational method in the pair approximation was applied to a study of the Ising ferromagnet with $S = 1$, $3/2$, 2, and $5/2$ in [3], where only the spontaneous magnetization was studied as a function of the reduced temperature for $S = 2$. The exact solution of the Ising model on a honeycomb lattice for $S = 3/2$ and 2 was obtained in [4] via a straightforward generalization of the method used in [5]. The mean-field solution of the Blume–Capel (BC) model for $S = 1$, $3/2$, 2, and 3 was investigated in [6]. Bifurcation diagrams for the set of ferromagnetic fixed points of the spin-2 BC model on a Cayley tree of coordination number $z = 3$ were presented in [7]. Two-spin cluster effective field theory for the BC model with spins $S = 1$, $3/2$, and 2 was developed and the phase diagrams were presented in [8]. It was also found there that the system exhibits a tricritical point for $S \geq 1$ and only if S is an integer, when the ratio D/J is less than -1. The magnetic properties of the spin-S (1, 2, and 3) Ising system with bilinear and biquadratic exchange interactions was investigated in [9] using the four-spin model approximation for a negative value of the biquadratic interaction. The temperature dependence of the dipole moment of the model for $S = 2$ was investigated and the ground state of the system was also discussed. On the other hand, the transverse Ising model with arbitrary spins S was studied in [10] for $S = 3/2$ and 2 and in [11] for $S = 1/2$, 1, $3/2$, 2, and $5/2$ within the

*E-mail: keskin@erciyes.edu.tr
**E-mail: canko@erciyes.edu.tr
***E-mail: mhmtertas@hotmail.com

effective field theory. Moreover, the properties of the spin-2 transverse Ising model have been investigated within the framework of the effective filed theory in detail [12–17]. The bimodal and trimodal random-field spin-2 Ising systems in a transverse field were studied by combining the pair approximation with the discretized path-integral representation [18, 19], and the matrix product approach was used to construct all optimum ground states of general anisotropic spin-2 chains with nearest-neighbor interactions and common symmetries [20]. Recently, the complete phase diagrams of the antiferromagnetic spin-2 Ising system were investigated on the Bethe lattice using the exact recurrence relations [21]. On the other hand, the zero-temperature phase diagram of a one-dimensional spin-2 Heisenberg ferromagnet was studied numerically using the density-matrix renormalization-group method [22], and spin-2 Heisenberg antiferromagnetic chains were also investigated by the Monte Carlo calculation [23]. Ground-state phase diagrams of the quantum spin-2 Ising model on the square lattice [24] and on the hexagonal lattice [25] were also constructed.

While the equilibrium properties of the spin-2 Ising model have been studied extensively, as far as we know, the nonequilibrim aspects of the spin-2 Ising model have not been investigated. The purpose of the present paper is therefore to present a study, within a mean-field approach, of the kinetics of the spin-2 BC model in the presence of a time-dependent oscillating external magnetic field. We use the Glauber-type stochastic dynamics to describe time evolution of the system [26]. Specifically, we investigate the time dependence of the average magnetization and the behavior of the dynamic order parameter as a function of the reduced temperature. In these studies, we obtain dynamical phase transition (DPT) points and construct phase diagrams in the reduced temperature and reduced magnetic field amplitude plane. This type of calculation was first applied to a kinetic spin-1/2 Ising system in [27] and then used to study kinetics of a classical mixed spin-1/2 and spin-1 Ising system in [28], and the kinetics of spin-1 Ising system in [29] and spin-3/2 [30] Ising systems in [30].

We also mention that the DPT has attracted much attention in recent years, theoretically [27–34] and from the standpoint of analytical studies [35]. Experimental evidences for the DPT have been found in magnetic systems [36] and amorphous YBaCuO films [37]. Moreover, besides the scientific interests, the study of DPT can inspire new methods in material manufacturing and processing, and interesting methods in nanotechnology, such as the pattern formation [38], monomolecular organic films [39], beam-induced transformation, and many others [40].

The outline of this paper is as follows. In Sec. 2, the spin-2 BC model is briefly described and the dynamic equation of motion is derived. In Sec. 3, DPT points are calculated and phase diagrams are presented. The paper ends with a summary and conclusion in Sec. 4.

2. THE MODEL AND DERIVATION OF MEAN-FIELD DYNAMIC EQUATIONS

The spin-2 BC model given by a spin-2 Ising Hamiltonian with a crystal-field interaction or single-ion anisotropy is defined by the Hamiltonian

$$\mathcal{H} = -J \sum_{\langle ij \rangle} S_i S_j - D \sum_i S_i^2 - H \sum_i S_i, \qquad (1)$$

where S_i takes the values ± 2, ± 1, and 0 at each site i of a lattice and $\langle ij \rangle$ denotes summation over all pairs of nearest-neighbor sites. J is the bilinear exchange interaction parameter, D is the crystal-field interaction or single-ion anisotropy, and H is a time-dependent external oscillating magnetic field given by

$$H(t) = H_0 \cos(wt). \qquad (2)$$

The system is in contact with an isothermal heat bath at an absolute temperature T_A.

The system evolves according to a Glauber-type stochastic process at a rate of $1/\tau$ transitions per unit time. We define $P(S_1, S_2, \ldots, S_N; t)$ as the probability that the system has the spins $S_1, S_2, \ldots, S_N$ at time t. The time dependence of this probability function is assumed to be governed by the master equation that describes the interaction between spins and the heat bath and can be written as

$$\begin{aligned}
\frac{d}{dt} P(S_1, S_2, \ldots, S_N; t) = \\
= -\sum_i \left(\sum_{S_i \neq S_i'} W_i(S_i \to S_i') \right) \times \\
\times P(S_1, S_2, \ldots, S_i, \ldots, S_N; t) + \\
+ \sum_i \left(\sum_{S_i \neq S_i'} W_i(S_i' \to S_i) \times \right. \\
\left. \times P(S_1, S_2, \ldots, S_i', \ldots, S_N; t) \right), \qquad (3)
\end{aligned}$$

where $W_i(S_i \to S_i')$ is the probability per unit time that the ith spin S changes from S_i to S_i', and in this sense the Glauber model is stochastic. Because the system is in contact with a heat bath at the absolute temperature T_A, each spin can change from the value S_i to the value S_i' with the probability per unit time given by

$$W_i(S_i \to S_i') = \frac{1}{\tau} \frac{\exp\left(-\beta \Delta E(S_i \to S_i')\right)}{\sum\limits_{S_i'} \exp\left(-\beta \Delta E(S_i \to S_i')\right)}, \qquad (4)$$

where $\beta = 1/k_B T_A$, $\sum\limits_{S_i'}$ is the sum over the five possible values ± 2, ± 1, 0 of S_i' and

$$\Delta E(S_i \to S_i') = \\ = -(S_i' \to S_i) \left(J \sum_{\langle j \rangle} S_j + H \right) - (S_i'^2 - S_i^2) D \qquad (5)$$

gives the change in the energy of the system when the S_i spin changes. The probabilities satisfy the detailed balance condition

$$\frac{W_i(S_i \to S_i')}{W_i(S_i' \to S_i)} = \frac{P(S_1, S_2, \ldots, S_i', \ldots, S_N)}{P(S_1, S_2, \ldots, S_i, \ldots, S_N)}. \qquad (6)$$

Substituting the possible values of S_i, we obtain

$$W_i(2 \to 0) = W_i(1 \to 0) = \\ = W_i(-1 \to 0) = W_i(-2 \to 0) = \\ = \frac{1}{\tau} \frac{1}{2\exp(\beta D)\operatorname{ch}(\beta a) + 2\exp(4\beta D)\operatorname{ch}(2\beta a) + 1}, \qquad (7a)$$

$$W_i(2 \to 1) = W_i(0 \to 1) = \\ = W_i(-1 \to 1) = W_i(-2 \to 1) = \\ = \frac{1}{\tau} \frac{\exp(\beta a)\exp(\beta D)}{2\exp(\beta D)\operatorname{ch}(\beta a) + 2\exp(4\beta D)\operatorname{ch}(2\beta a) + 1}, \qquad (7b)$$

$$W_i(1 \to 2) = W_i(0 \to 2) = \\ = W_i(-1 \to 2) = W_i(-2 \to 2) = \\ = \frac{1}{\tau} \frac{\exp(2\beta a)\exp(4\beta D)}{2\exp(\beta D)\operatorname{ch}(\beta a) + 2\exp(4\beta D)\operatorname{ch}(2\beta a) + 1}, \qquad (7c)$$

$$W_i(1 \to -1) = W_i(2 \to -1) = \\ = W_i(0 \to -1) = W_i(-2 \to -1) = \\ = \frac{1}{\tau} \frac{\exp(-\beta a)\exp(\beta D)}{2\exp(\beta D)\operatorname{ch}(\beta a) + 2\exp(4\beta D)\operatorname{ch}(2\beta a) + 1}, \qquad (7d)$$

$$W_i(2 \to -2) = W_i(1 \to -2) = \\ = W_i(0 \to -2) = W_i(-1 \to -2) = \\ = \frac{1}{\tau} \frac{\exp(-2\beta a)\exp(4\beta D)}{2\exp(\beta D)\operatorname{ch}(\beta a) + 2\exp(4\beta D)\operatorname{ch}(2\beta a) + 1}, \qquad (7e)$$

where

$$a = J \sum_{\langle j \rangle} S_j + H.$$

We note that because $W_i(S_i \to S_i')$ is independent of S_i, we can write $W_i(S_i \to S_i') = W_i(S_i')$, and the master equation becomes

$$\frac{d}{dt} P(S_1, S_2, \ldots, S_N; t) = -\sum_i \left(\sum_{S_i \neq S_i'} W_i(S_i') \right) \times \\ \times P(S_1, S_2, \ldots, S_i, \ldots, S_N; t) + \sum_i W_i(S_i) \times \\ \times \left(\sum_{S_i \neq S_i'} P(S_1, S_2, \ldots, S_i', \ldots, S_N; t) \right). \qquad (8)$$

Because the sum of probabilities is normalized to one, multiplying both sides of Eq. (8) by S_k and taking the average we obtain

$$\tau \frac{d}{dt} \langle S_k \rangle = -\langle S_k \rangle + \frac{2\exp(4\beta D)\operatorname{sh}\left[2\beta\left(J\sum\limits_{\langle j \rangle} S_j + H\right)\right] + \exp(\beta D)\operatorname{sh}\left[\beta\left(J\sum\limits_{\langle j \rangle} S_j + H\right)\right]}{\exp(4\beta D)\operatorname{ch}\left[2\beta\left(J\sum\limits_{\langle j \rangle} S_j + H\right)\right] + \exp(\beta D)\operatorname{ch}\left[\beta\left(J\sum\limits_{\langle j \rangle} S_j + H\right)\right] + 1/2}, \qquad (9)$$

or, in terms of the mean-field approach,

$$\tau \frac{d}{dt} \langle S \rangle = -\langle S \rangle + \frac{2\exp(4\beta D)\operatorname{sh}\left[2\beta\left(Jz\langle S \rangle + H_0\cos(wt)\right)\right] + \exp(\beta D)\operatorname{sh}\left[\beta\left(Jz\langle S \rangle + H_0\cos(wt)\right)\right]}{\exp(4\beta D)\operatorname{ch}\left[2\beta\left(Jz\langle S \rangle + H_0\cos(wt)\right)\right] + \exp(\beta D)\operatorname{ch}\left[\beta\left(Jz\langle S \rangle + H_0\cos(wt)\right)\right] + 1/2}, \qquad (10)$$

where z is the coordination number for this model. The system evolves according to differential equation (10), which can be written as

$$\Omega \frac{d}{d\xi} m = -m + \frac{2\exp(4d/T)\operatorname{sh}\left[(2/T)(m + h\cos\xi)\right] + \exp(d/T)\operatorname{sh}\left[(1/T)(m + h\cos\xi)\right]}{\exp(4d/T)\operatorname{ch}\left[(2/T)(m + h\cos\xi)\right] + \exp(d/T)\operatorname{ch}\left[(1/T)(m + h\cos\xi)\right] + 1/2}, \qquad (11)$$

where $m = \langle S \rangle$, $\xi = wt$, $T = (\beta z J)^{-1}$, $d = D/zJ$, $h = H_0/zJ$, and $\Omega = \tau w$. We fixed $z = 4$ and $\Omega = 2\pi$. A solution and a discussion of this equation are given in the next section.

3. DYNAMIC PHASE TRANSITION POINTS AND PHASE DIAGRAMS

In this section, we find the DPT points and present the phase diagrams. For this, we first have to study stationary solutions of dynamic equation (11), when the parameters T, d, and h are varied. The stationary solution of Eq. (11) is a periodic function of ξ with period 2π, $m(\xi + 2\pi) = m(\xi)$. Moreover, they can be one of two types according to whether they have or do not have the property

$$m(\xi + \pi) = -m(\xi). \tag{12}$$

A solution that satisfies Eq. (12) is called symmetric; it corresponds to a paramagnetic (P) phase. In this solution, the magnetization $m(\xi)$ oscillates around the zero value and is delayed with respect to the external field. Solutions of the second type, which do not satisfy Eq. (12), are called nonsymmetric; they correspond to a ferromagnetic (F) phase. In this case the magnetization does not follow the external magnetic field any more but instead oscillates around a nonzero value, ± 2 or ± 1. If it oscillates around ± 2, it corresponds to the ferromagnetic-2 (F_2) phase and if it oscillates around ± 1, it corresponds to the ferromagnetic-1 (F_1) phase. These facts are seen explicitly by solving Eq. (11) numerically.

Equation (11) is solved numerically using the Adams–Moulton predictor corrector method for a given set of parameters and initial values. The results are presented in Fig. 1. From Fig. 1, we can see five different solutions: P, F_2, and three coexistence solutions, namely, F_2 + P, F_1 + P, and F_2 + F_1 + P. In Fig. 1*a*, only the symmetric solution is always obtained, and hence we have a paramagnetic (P) solution, but in Fig. 1*b*, only the nonsymmetric solutions are found, and we therefore have a ferromagnetic (F_2) solution. These solutions do not depend on the initial values. On the other hand, in Fig. 1*c*, both the F_2 and P phases always exist in the system, and hence we have the coexistence solution (F_2 + P). In this case, the solutions depend on the initial values, as can be seen in Fig. 1*c* explicitly. Figures 1*d*–*e* are similar to Fig. 1*c*, except that F_1 and P phases exist in Fig. 1*d* and F_2, F_1, and P phases exist in Fig. 1*e*. Therefore, we have three different coexistence solutions, which depend on the initial values.

To obtain the dynamic phase boundaries between these five phases or regions in Fig. 1, we have to calculate DPT points, which then allow us to present phase diagrams of the system. DPT points are obtained by investigating the behavior of the average magnetization in a period as a function of the reduced temperature.

The average magnetization (M) in a period, which is also called the dynamic magnetization, is given by

$$M = \frac{1}{2\pi} \int_0^{2\pi} m(\xi)\, d\xi. \tag{13}$$

The behavior of M as a function of the reduced temperature for several values of h and d is obtained by combining the numerical Adams–Moulton predictor corrector method with the Romberg integration. We give a few interesting examples to illustrate the calculation of the DPT and the dynamic phase boundaries between the five phases, seen in Fig. 2. In Fig. 2, T_C and T_t are a critical (or second-order) phase transition and a first-order phase transition temperatures, respectively. Figure 2*a* shows the behavior of M as a function of the reduced temperature for $d = 1.0$ and $h = 0.5$. At zero temperature, $M = 2.0$; M decreases to zero continuously as the reduced temperature T increases, and therefore the system undergoes a second-order phase transition at $T_C = 2.2292$, the transition being from the F_2 phase to the P phase. Figure 2*b* displays the behavior of M as a function of the reduced temperature for $d = 1.0$ and $h = 1.375$. At zero temperature, $M = 2.0$; M decreases to zero discontinuously as the reduced temperature increases, and therefore a first-order phase transition occurs. The first-order phase transition temperature $T_t = 1.1975$ is marked with a dashed arrow in Fig. 2. Figures 2*c* and 2*d* illustrate the thermal variations of M for $d = -1.3$ and $h = 0.0125$ for two different initial values of M: 2.0 or 1.0 in Fig. 2*c* and zero in Fig. 2*d*. In Fig. 2*c*, the system exhibits a second-order phase transition from the F_2 phase to the P phase. In Fig. 2*d*, the system undergoes two successive phase transitions: the first is a first-order one at $T_t = 0.122$, the transition being from the P phase to the F_2 phase, and the second is a second-order phase transition at $T_C = 1.418$ from the F_2 phase to the P phase. This means that the F_2 + P coexistence region exists for $d = -1.3$ and $h = 0.0125$ in the system. This fact is seen in the phase diagram in Fig. 3*c* explicitly (compare Figs. 2*c* and 2*d* with Fig. 3*c* for $h = 0.0125$). Figures 2*e*–*g* illustrate the thermal variation of M for $d = -2.25$ and $h = 0.175$ for three different initial values of M: 2.0 in Fig. 2*e*, 1.0 in Fig. 2*f*, and zero in Fig. 2*g*. Figure 2*e* shows that the system undergoes

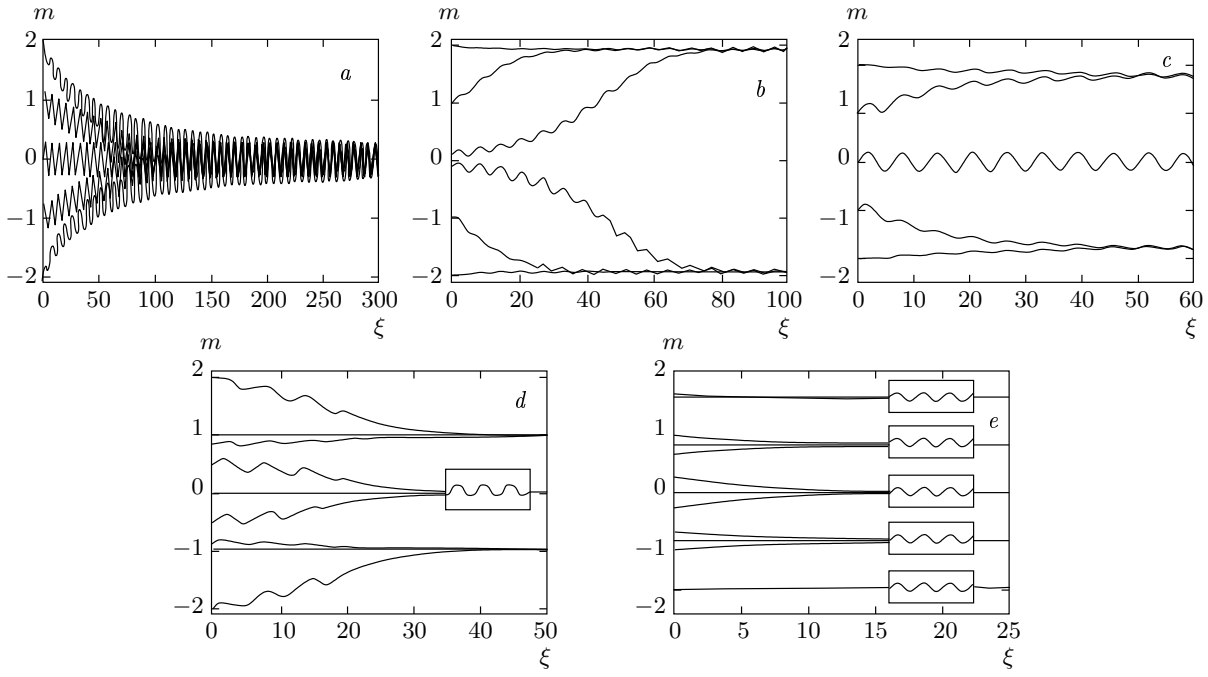

Fig. 1. Time variations of the average magnetization (m). *a*) Exhibiting a paramagnetic phase (P), $d = 1.0$, $h = 1.425$, and $T = 1.5$. *b*) Exhibiting a ferromagnetic-2 (F_2) phase, $d = -1.5$, $h = 0.4$, and $T = 0.25$. *c*) Exhibiting a coexistence region (F_2 + P), $d = -1.5$, $h = 0.86$, and $T = 0.625$. *d*) Exhibiting a coexistence region (F_1 + P), $d = -2.25$, $h = 0.325$, and $T = 0.0375$. *e*) Exhibiting a coexistence region (F_2 + F_1 + P), $d = -2.25$, $h = 0.2325$, and $T = 0.0275$

two successive first-order phase transitions; the first is from the F_2 phase to the F_1 phase at $T_t = 0.0617$ and the second is from the F_1 phase to the P phase at $T_t = 0.1575$. In Fig. 2*f*, the system undergoes a first-order phase transition from the F_1 phase to the P phase at $T_{t'} = 0.1575$. Figure 2*g* illustrates that the system does not undergo any phase transitions, but the P phase always exists for these values. Therefore, the F_2 + F_1 + P coexistence region occurs below $T_{t'} = 0.1575$, and the F_1 + P region exists between $T_t = 0.0617$ and $T_{t'} = 0.1575$, and the P phase occurs above $T_{t'} = 0.1575$. This fact is also seen in the phase diagram in Fig. 3*e* explicitly (compare Figs. 2*e–g* with Fig. 3*e* for $h = 0.175$).

We can now obtain phase diagrams of the system. The calculated phase diagrams in the (T, h) plane are presented in Fig. 3. The solid and dashed lines respectively represent the second- and first-order phase transition lines and the dynamic tricritical point is denoted by a solid circle. As seen in Fig. 3, we have obtained seven different phase-diagram topologies.

(i) For $d \geq -0.265$, Fig. 3*a* displays the phase diagram in the (T, h) plane for $d = 1.0$. In this phase diagram, the solutions are paramagnetic (P) for the higher reduced temperatures T and reduced external magnetic field amplitudes h, and ferromagnetic-2 (F_2) for low values of T and h. The dynamic phase boundary between these regions, $F_2 \to P$, is a second-order phase transition line. For low reduced temperatures, there is a range of values of h where the P and F_2 phases coexist, called the coexistence region, F_2 + P. The F_2 + P region is separated from the F_2 and P phases by a first-order phase transition line. The system also exhibits only one dynamic tricritical point where both first-order phase transition lines merge, which signals a change from a first-order to a second-order phase transitions. Finally, we mention that similar phase diagrams have also been obtained in the kinetic spin-1/2 Ising [27], spin-1 Ising [29] and spin-3/2 Ising [30] systems.

(ii) For $-0.265 > d \geq -1.043$, we have presented the phase diagram at $d = -1.0$ in Fig. 3*b*. This phase diagram is similar to the one in Fig. 3*a*, but differs from it in that at low values of T and h, one more F_2 + P coexistence region exists. The dynamic phase boundary between this F_2 + P region and the F_2 phase is a first-order line. A similar phase diagram has also been obtained for the spin-1 Ising systems [29], except that the ferromagnetic phase is F_2 instead of F_1.

(iii) For $-1.043 > d \geq -1.426$, the phase diagram

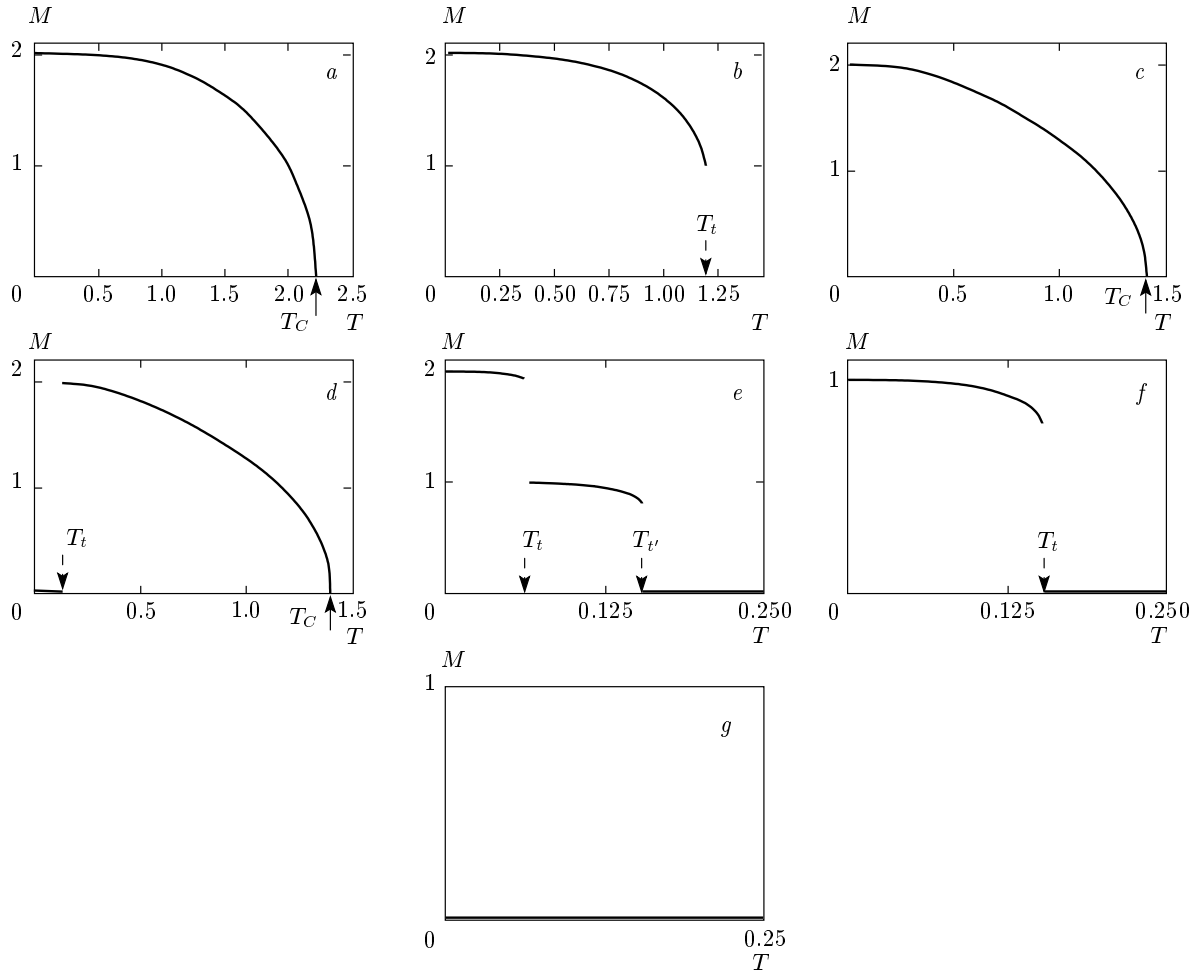

Fig. 2. The reduced temperature dependence of the dynamic magnetization M. T_C and T_t are respectively the second-order phase transition and the first-order phase transition temperatures. *a*) A second-order phase transition from the F_2 phase to the P phase for $d = 1.0$ and $h = 0.50$; 2.2292 is found for T_C. *b*) A first-order phase transition from the F_2 phase to the P phase for $d = 1.0$ and $h = 1.375$; 1.1975 is found for T_t. *c*) A second-order phase transition from the F_2 phase to the P phase for $d = -1.3$ and $h = 0.0125$; 1.418 is found for T_C. *d*) Two successive phase transitions, a first-order phase transition from the P phase to the F_2 phase and a second-order phase transition from the F_2 phase to the P phase for $d = -1.3$ and $h = 0.0125$; 0.122 and 1.4042 are found for T_t and T_C, respectively. *e*) Two successive first-order phase transitions, the first from the F_2 phase to the F_1 phase and the second from the F_1 phase to the P phase for $d = -2.25$ and $h = 0.175$; 0.0617 and 0.1575 are found for T_t and $T_{t'}$, respectively. *f*) The same as in Fig. 2*b*, but with the first-order phase transition from the F_1 phase to the P phase, for $d = -2.25$ and $h = 0.175$; 0.1575 is found for $T_{t'}$. *g*) The system does not undergo any phase transition, $d = -2.25$ and $h = 0.175$

is shown for $d = -1.3$ in Fig. 3*c*. It is similar to case (ii), with the following differences. 1) One more F_2 + P phase occurs for low values of T and high values of h and the dynamic boundary between this coexistence phase and the F_2 phase is also a first-order line. 2) The F_2 + P phase, which exists for very high values of h, becomes the F_1 + P phase. A similar phase diagram has also been found for the spin-3/2 Ising systems, except that the ferromagnetic phase is F_2 instead of $F_{3/2}$.

(iv) For $-1.426 > d \geq -1.957$, the phase diagram is presented for $d = -1.5$ in Fig. 3*d*. The phase diagram is similar to the one in Fig. 3*b*, with the following differences. 1) For very low values of T and h, the F_2 + F_1 + P coexistence region occurs. 2) The F_2 + P phase, which exists for very high values of h, becomes the F_1 + P phase. The dynamic phase boundary between the F_2 + F_1 + P phase and F_1 + P phase is also a first-order phase transition line.

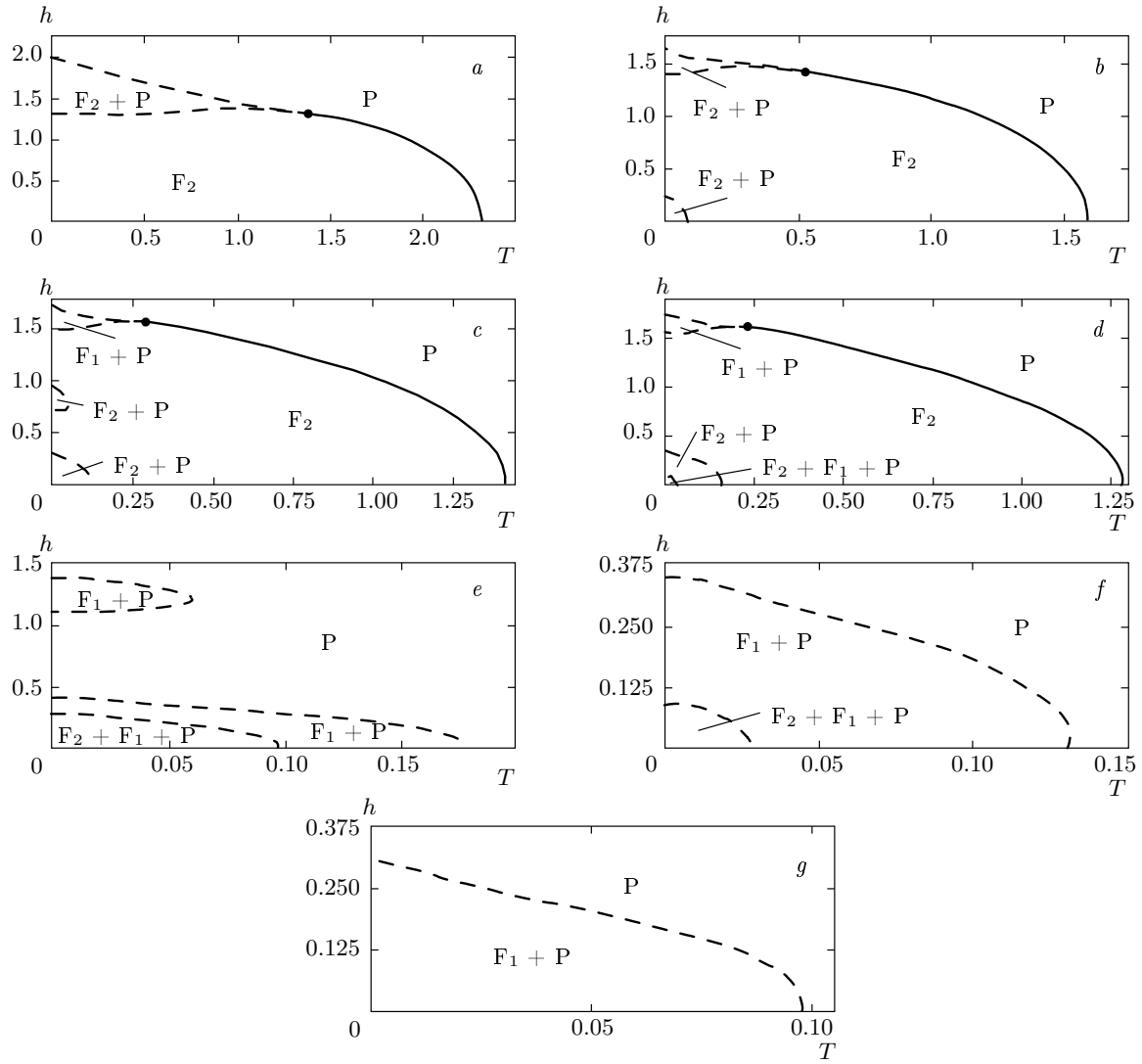

Fig. 3. Phase diagrams of the spin-2 BC model in the (T, h) plane. The Paramagnetic (P), Ferromagnetic-2 (F_2), and three different coexistence (F_2 + P, F_1 + P, F_2 + F_1 + P) regions are found. Dashed and solid lines respectively represent the first- and second-order phase transitions, and the dynamic tricritical point is indicated with solid circles. $d = 1.0$ (a), -1.0 (b), -1.3 (c), -1.5 (d), -2.25 (e), -2.5 (f), and -2.75 (g)

(v) For $-1.957 > d \geq -2.364$, the phase diagram is shown in Fig. 3*e* for $d = -2.25$. This phase diagram is similar to Fig. 3*d*, except for the following differences. 1) The second-order phase transition line disappears; hence, the system does not exhibit a dynamic tricritical point. 2) The F_2 phase also disappears.

(vi) For $-2.364 > d \geq -2.587$, the phase diagram is constructed for $d = -2.50$ in Fig. 3*f*. It is similar to Fig. 3*e* but differs from it in that the F_1 + P coexistence region, which appears for very low values of T and high values of h, now disappears.

(vii) For $-2.587 > d$, the phase diagram is similar to the one in Fig. 3*f* but differs from it in that for very low values of T and h, the F_2 + F_1 + P region disappears, as illustrated in Fig. 3*g*.

4. SUMMARY AND CONCLUSION

Within a mean-field approach, we have presented a study of the stationary states of the kinetic spin-2 BC model and its kinetics described by the Glauber-type stochastic dynamics in the presence of a time-dependent oscillating external magnetic field. We have studied the time dependence of the average magnetiza-

tion and the behavior of the average magnetization in a period. The DPT points are found by investigating the behavior of the dynamic magnetization as a function of the reduced temperature.

We also mention that a phase diagram similar to the one in Fig. 3*a* has been obtained for kinetic spin-1/2 Ising model [27], the kinetic spin-1 Ising model [29], and kinetic spin-3/2 Ising model [30], but a phase diagram similar to Fig. 3*b* has been found only in kinetic spin-1 Ising systems [29]. The five phase diagrams in Fig. 3*c, d, e, f,* and *g* are a new type of phase diagrams, which have been only obtained in the kinetic spin-2 BC model in the presence of a time-dependent oscillating magnetic field by using the Glauber-type stochastic dynamics. The phase diagrams exhibit one dynamic tricritical point, the P and F_2 phases, and the F_2 + P, F_1 + P, and F_2 + F_1 + P coexistence phase regions, which strongly depend on the interaction parameter.

Finally, it is worthwhile to mention that there is a strong possibility that at least some of the first-order transitions and multicritical points seen in the mean-field results are artefacts of the approximation. This is because for the field amplitude less than the coercive field (at the temperature less than the static ferro–para (or order–disorder) transition temperature), the response magnetization varies periodically but asymmetrically even in the zero-frequency limit; the system may remain locked to one well of the free energy and cannot go to another well, in the absence of noise or fluctuations [31–34]. However, this mean-field dynamic study suggests that the spin-2 BC model has an interesting dynamic behavior and gives rich dynamic phase diagrams. Hence, we hope that our detailed investigation may stimulate further works to study the DPT in the kinetic spin-2 model theoretically by using more accurate techniques such as dynamic Monte Carlo simulations or renormalization group calculations.

This work was supported by the Scientific and Technological Research Council of Turkey (TÜBİTAK), (Grant №105T114), and Erciyes University Research Funds (Grant № FBA-06-01). We are very grateful to B. Deviren, M. Kırak, and E. Kantar for useful discussions.

REFERENCES

1. T. Obokata and T. Oguchi, J. Phys. Soc. Japan **25**, 322 (1968).
2. D. K. Ray and J. Sivardiére, Phys. Rev. B **18**, 1401 (1978).
3. J. W. Tucker, J. Magn. Magn. Mater. **71**, 27 (1987).
4. A. Lipowski and M. Suzuki, Physica A **193**, 360 (1993).
5. M. Kolesik and L. Šamaj, Int. J. Mod. Phys. B **6**, 1529 (1992).
6. J. A. Plascak, J. G. Moreira, and F. C. Sá Berreto, Phys. Lett. A **173**, 360 (1993).
7. M. N. Tamashiro and S. R. A. Salinas, Physica A **211**, 124 (1994).
8. M. Jurčišin, A. Bobák, and M. Jaščur, Physica A **224**, 684 (1996).
9. T. Iwashita, R. Satou, T. Imada, and T. Idogaki, Physica B **248–288**, 1203 (2000).
10. T. Kaneyoshi, M. Jaščur, and I. P. Fittipaldi, Phys. Rev. B **48**, 250 (1993).
11. A. Elkouraychi, M. Saber, and J. W. Tucker, Physica A **217**, 576 (1995).
12. M. Saber and J. W. Tucker, Physica A **217**, 407 (1995).
13. H. El Mir, M. Saber, and J. W. Tucker, J. Magn. Magn. Mater. **138**, 76 (1994).
14. W. Jiang, G.-Z. Wie, and Z.-H. Xin, Phys. Stat. Sol. (b) **225**, 215 (2001).
15. W. Jiang, G.-Z. Wie, D. An, and Z. Qi, Chinese Phys. **11**, 832 (2002).
16. Y.-Q. Liang, G.-Z. Wei, Q. Zang, and G.-I. Song, Chinese Phys. Lett. **21**, 378 (2002).
17. Y.-Q. Liang, G.-Z. Wei, L.-L. Song, and S.-L. Zang, Comm. Theor. Phys. **42**, 623 (2004).
18. O. Canko, E. Albayrak, and M. Keskin, J. Magn. Magn. Mater. **294**, 63 (2005).
19. O. Canko and E. Albayrak, Phys. Lett. A **340**, 18 (2005).
20. M. A. Ahrens, A. Schadschneider and J. Zittartz, Europhys. Lett. **59**, 889 (2002).
21. A. Erdinç, O. Canko, and E. Albayrak, Europ. Phys. J. B **52**, 521 (2006).
22. M. Dudzinski, G. Fath, and J. Sznajd, Phys. Rev. B **59**, 13764 (1999).
23. G. Sun, Phys. Rev. B **51**, 8370 (1995).
24. H. Niggemann, A. Klümper, and J. Zittartz, Europ. Phys. J. B **13**, 15 (2000).

25. M. A. Ahrens, A. Schadschneider, and J. Zittartz, Phys. Rev. B **71**, 174432 (2005).

26. R. J. Glauber, J. Math. Phys. **4**, 294 (1963).

27. T. Tomé and M. J. de Oliveira, Phys. Rev. A **41**, 4251 (1990).

28. G. M. Buendía and E. Machado, Phys. Rev. E **58**, 1260 (1998).

29. M. Keskin, O. Canko, and Ü. Temizer, Phys. Rev. E **72**, 036125 (2005); M. Keskin, O. Canko, and E. Kantar, Int. J. Mod. Phys. C **17**, 1239 (2006); O. Canko, Ü. Temizer, and M. Keskin, *ibid*, **17**, 1717 (2006); M. Keskin, O. Canko, and Ü. Temizer, Zh. Eksp. Teor. Fiz. **134**, 1073 (2007); M. Keskin, Ü. Temizer, O. Canko, and E. Kantar, Phase Trans. **80**, 855 (2007).

30. M. Keskin, O. Canko, and B. Deviren, Phys. Rev. E **74**, 011110 (2006); O. Canko, B. Deviren, and M. Keskin, J. Phys.: Condens. Matter **18**, 6635 (2006); M. Keskin, O. Canko, and B. Deviren, J. Magn. Magn. Mater. **313**, L1 (2006); M. Keskin, O. Canko, and M. Kırak, J. Stat. Phys. **127**, 359 (2007).

31. M. Acharyya, Phys. Rev. E **56**, 2407 (1997); A. Chatterjee and B. K. Chakrabarti, Phys. Rev. E **67**, 046113 (2003).

32. S. W. Sides, P. A. Rikvold, and M. A. Novotny, Phys. Rev. Lett. **81**, 834 (1998); S. W. Sides, P. A. Rikvold, and M. A. Novotny, Phys. Rev. E **59**, 2710 (1999); G. Korniss, C. J. White, P. A. Rikvold, and M. A. Novotny, Phys. Rev. E **63**, 016120 (2001); G. Korniss, P. A. Rikvold, and M. A. Novotny, Phys. Rev. E **66**, 056127 (2002).

33. B. K. Chakrabarti and M. Acharyya, Rev. Mod. Phys. **71**, 847 (1999); M. Acharyya, Int. J. Mod. Phys. C **16**, 1631 (2005).

34. M. F. Zimmer, Phys. Rev. E **47**, 3950 (1993); M. Acharyya and B. K. Chakrabarti, Phys. Rev. B **52**, 6550 (1995); M. Acharyya, Phys. Rev. E **58**, 179 (1998).

35. H. Fujisaka, H. Tutu, and P. A. Rikvold, Phys. Rev. E **63**, 036109 (2001); **63**, 059903 (E); H. Tutu and N. Fujiwara, J. Phys. Soc. Jpn. **73**, 2680 (2004); E. Z. Meilikov, Pis'ma v Zh. Eksp. Teor. Fiz. **79**, 757 (2004).

36. Q. Jiang, H. N. Yang, and G. C. Wang, Phys. Rev. B **52**, 14911 (1995); W. Kleemann, T. Braun, J. Dec, and O. Petracic, Phase Trans. **78**, 811 (2005); D. T. Robb, Y. H. Xu, O. Hellwing, A. Berger, M. A. Novotny, and P. A. Rikvold, Meeting Amer. Phys. Soc. Baltimore, USA (2006); D. T. Robb, Y. H. Xu, O. Hellwing, J. McCord, A. Berger, M. A. Novotny, and P. A. Rikvold, to be submitted to Phys. Rev. B (2007).

37. Z. A. Samoilenko, V. D. Okunev, E. I. Pushenko, V. A. Isaev, P. Gierlowski, K. Kolwas, and S. J. Lewandowski, Inorg. Mater. **39**, 836 (2003).

38. M. C. Cross and P. C. Hohenberg, Rev. Mod. Phys. **65**, 851 (1993).

39. A. S. Mikhailov and G. Ertl, Science **272**, 1596 (1996).

40. E. Ma, P. Bellon, M. Atzmon, and R. Tivedi, eds., *Phase Transformations and Systems Driven Far from Equilibrium*, Mater. Res. Soc. Symp. Proc., Vol. **481** (1998).